Velocity dependence of heavy-ion stopping below the maximum

Sigmund, Peter; Schinner, Andreas

Published in:
Nuclear Instruments & Methods in Physics Research. Section B: Beam Interactions with Materials and Atoms

Publication date:
2015

Document version
Submitted manuscript

Citation for pulished version (APA):
Sigmund, P., & Schinner, A. (2015). Velocity dependence of heavy-ion stopping below the maximum. Nuclear Instruments & Methods in Physics Research. Section B: Beam Interactions with Materials and Atoms, 342(1), 292-299.

Velocity Dependence of Heavy-Ion Stopping below the Maximum

P. Sigmund[a], A. Schinner[b]

[a]*Department of Physics, Chemistry and Pharmacy, University of Southern Denmark, DK-5230 Odense M, Denmark*
[b]*Institut für Experimentalphysik, Johannes Kepler Universität, A-4040 Linz, Austria*

Abstract

In the slowing-down of heavy ions in materials, the standard desription by Lindhard and Scharff assumes the electronic stopping cross section to be proportional to the projectile speed v up to close to a stopping maximum, which is related to the Thomas-Fermi speed v_{TF}. It is well known that strict proportionality with v is rarely observed, but little is known about the systematics of observed deviations. In this study we try to identify factors that determine positive or negative curvature of stopping cross sections on the basis of experimental data and of binary stopping theory. We estimate the influence of shell structure of the target and of the equilibrium charge of the ion and comment the role of dynamics screening.

Keywords: Stopping power, Stopping force, Swift heavy ions, Ion charge, Low-velocity stopping

1. Introduction

In the characterization of the slowing down of ions in matter it is customary to talk about the velocity-proportional regime, when the projectile speed v lies well below the Thomas-Fermi speed $v_{\rm TF} = Z_1^{2/3} v_0$, where Z_1 is the atomic number of the projectile and v_0 the Bohr speed [1]. This classification, proposed by Lindhard and Scharff [2], is one of the corner stones in the theory of ion implantation [3] and ion-beam-induced radiation effects [4].

The assertion of approximately velocity-proportional *electronic stopping* is supported by evidence from range measurements, although deviations from strict proportionality are well known: Fastrup et al. [5] parameterized measured electronic stopping cross sections in the velocity regime around v_0 by a power law, $S \propto E^p$, where E is the ion energy and p a coefficient dependent on the ion-target combination that may differ noticeably from 0.5. Moak and Brown [6, 7] found stopping cross sections for heavy ions linear in v at velocities well above v_0, but when extrapolated to lower speeds, those straight lines pointed at an apparent nonvanishing threshold velocity. Empirical tabulations of stopping cross sections [8, 9] show significant deviations from velocity-proportional stopping.

The assumption of velocity-proportional electronic stopping draws support from numerous theoretical studies initiated by Fermi and Teller [10], Lindhard [11, 12] and Firsov [13, 14]. Strictly speaking, these theoretical schemes imply ion speeds significantly below the lowest electron speed in the target material or, roughly spoken, $v \ll v_0$. General theoretical arguments suggesting to extend this regime up to near the Thomas-Fermi speed have not been proposed to our knowledge. This is remarkable in view of the fact that the ratio $v_{\rm TF}/v_0$ can be as high as ~ 20 for heavy ions.

Recently, Lifschitz and Arista [15] asserted the observation of an apparent velocity threshold to be a consequence of dynamical screening and increasing equilibrium charge. In an attempt to theoretically reproduce experimental results by Brown and Moak [7], an apparent threshold was indeed found when stopping cross sections calculated for higher energies were extrapolated to lower energies. Calculations were performed for Br, I and U ions in C. While this work is interesting, it raises several questions:

- Is the behavior observed by Brown and Moak typical for heavy-ion stopping?
- Why do the calculations by Lifschitz and Arista overestimate measured stopping crosss sections, even though not all contributions to stopping are taken into account in the calculations?
- What is the role of the target shells?

The matter is important in our opinion both from a practical and a fundamental point of view. Measured stopping cross sections in the low-energy range are only available for a small fraction of all ion-target combinations (Z_1, Z_2), and the scatter between different data sets is significant and occasionally dramatic. Tabulations are based on interpolation [8, 9], for which the use of guiding principles such as reciprocity [16, 17] is desirable.

In the present work we first try to extract general features from available experimental data. Instead of dis-

Email address: sigmund@sdu.dk (P. Sigmund)

cussing apparent thresholds – which, to our knowledge, never have been asserted to represent real thresholds – we shall talk about deviations from velocity-proportional stopping in terms of positive or negative curvature. Lifschitz and Arista found that in a linear-linear plot versus speed, stopping cross sections follow an S-shaped curve starting with a linear portion at the low-v end, followed up by an interval with positive curvature, a quasilinear regime and, finally, a bend-over to negative curvature towards the stopping peak.

Following up on this we perform calculations with our PASS code that implements binary stopping theory [18] to study primarily the effects of target shells and ion charge on the curvature of the stopping cross section.

2. Experimental Findings

Figure 1 shows experimental data by Brown and Moak [7] – which formed the basis for the analysis by Lifschitz and Arista [15] – plotted together with other data for Br, I and U ions penetrating through C. The case of Br (upper graph) shows a rather consistent behavior of four data sets. The low-energy data by Hvelplund [19] are consistent with velocity proportionality, the bend-over toward a higher slope is covered by Zhang et al. [20]. Those data agree with Brown and Moak in the overlap regime. The latter data bend over toward negative curvature, where they are consistent with Anthony [21].

For iodine ions the scatter between data sets is larger than in Br-C at all energies. Nevertheless, despite the absence of low-v data it is clear that a behavior similar to Br-C must be expected. Uranium ions show a similar behavior, although the change in slope at $v/v_{TF} \simeq 0.2$ appears more abrupt than what has been found in the two former cases.

Figure 2 shows two combinations with Al as a target. For I-Al (upper graph) different conclusions can be drawn, dependent on which data are trusted: The data of Zhang et al. [20] together with those of Anthony and Lanford [21] resemble the Br-C case in figure 1. Conversely, the data of Bridwell et al. [22] indicate a linear velocity dependence up to the turn-over to negative curvature. For Au-Al (lower graph), existing data seem too scarce to allow conclusions without reference to theory or scaling relations.

Figure 3 shows ion-target combinations where no evidence is seen for a positive curvature. For H-C, actually a negative curvature is observed. For Cl-C and Ar-C a straight-line dependence is found up to $v/v_{TF} \simeq 0.6$, although there is considerable scatter in the case of Ar-C. This upper limit fits into the trend seen in figure 1. For Kr-C, a linear dependence can be extracted up to $v/v_{TF} \sim 0.4$, although data are missing in the interval between $v/v_{TF} \simeq 0.1$ and 0.3.

As a result of this preliminary survey we may conclude that there are significant deviations from the behavior of the data by Brown and Moak, both in competing data on the same ion-target combinations and on other ion-target

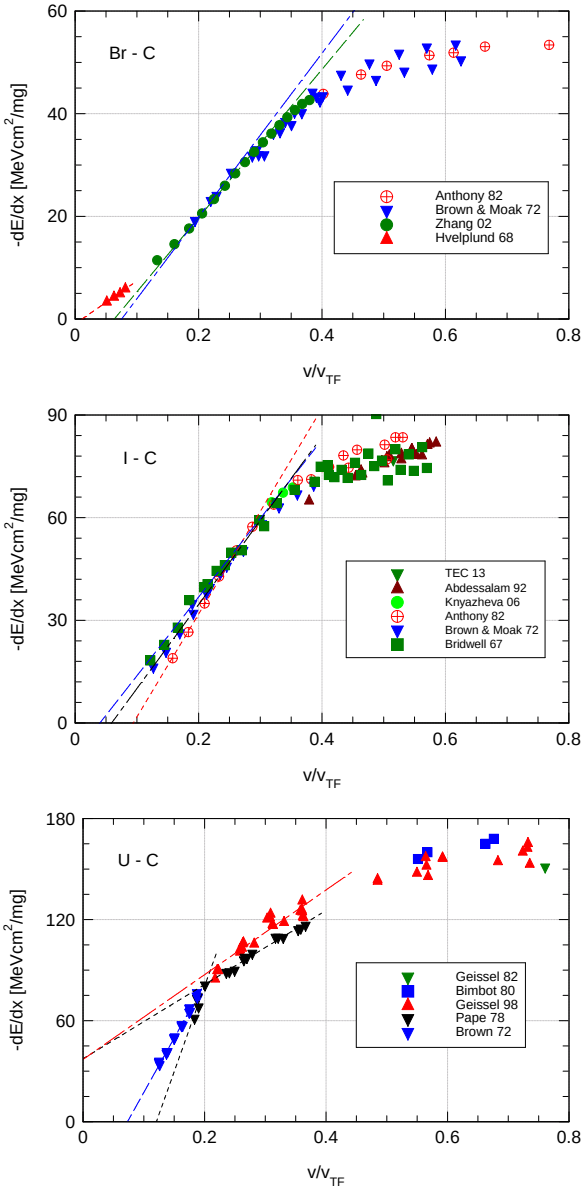

Figure 1: *Color on screen.* Measured stopping forces of C on Br, I and U ions, compiled by Paul [9]. Original data from refs. [7, 19–21, 21–29]. Dotted and stippled straight lines represent extrapolations from experimental data. Abscissa variable is the Thomas-Fermi speed $v_{TF} = Z_1^{2/3} v_0$.

combinations. In view of incomplete coverage with data, theory is needed to arrive at more definitive conclusions.

3. Nuclear Stopping

It appears essential at this point to discuss the role of nuclear stopping. Figure 4 shows nuclear and electronic stopping cross sections for I-Al according to refs. [3, 8]. It is seen that the contribution of nuclear stopping to the total stopping force is almost negligible in the quasi-linear velocity range above $v/v_{TF} \sim 0.15$, whereas this contribution is dominating below $v/v_{TF} < 0.05$.

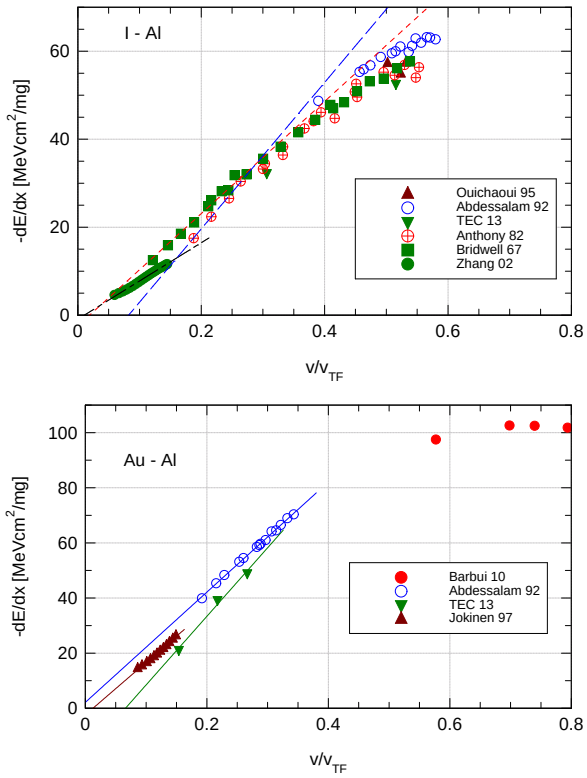

Figure 2: *Color on screen.* Same as figure 1 for I-Al and Au-Al. Original data from [20–22, 24, 25, 30–32].

In a previous study [44] it was pointed out that corrections for nuclear stopping were performed in different ways by different authors and, with very few exceptions, insufficiently documented. There are at least two major uncertainties:

- Nuclear energy loss is accompanied by angular deflection. For a narrow detection angle the effective nuclear stopping cross section will, therefore, be smaller than the full nuclear stopping cross section [5].

- Interatomic potentials and, hence, nuclear stopping cross sections involving very heavy ions, are poorly known.

For heavy ions, when the ion mass exceeds the target mass, angular deflection is a weak effect, so that the correction for nuclear stopping will come close to the full nuclear stopping cross section. As far as the contributions in figures 1-3 are concerned, corrections for nuclear stopping have been applied by the authors of refs. [6, 7, 19, 22]. In refs. [20, 21], such corrections were not mentioned and presumably not performed. This suggests that electronic stopping cross sections of Zhang et al. [20] are smaller than the total stopping cross sections shown in figure 2. For the data from ref. [21] the correction is presumably quite small. The remaining experimental data in figures 1-2 are barely affected by nuclear stopping.

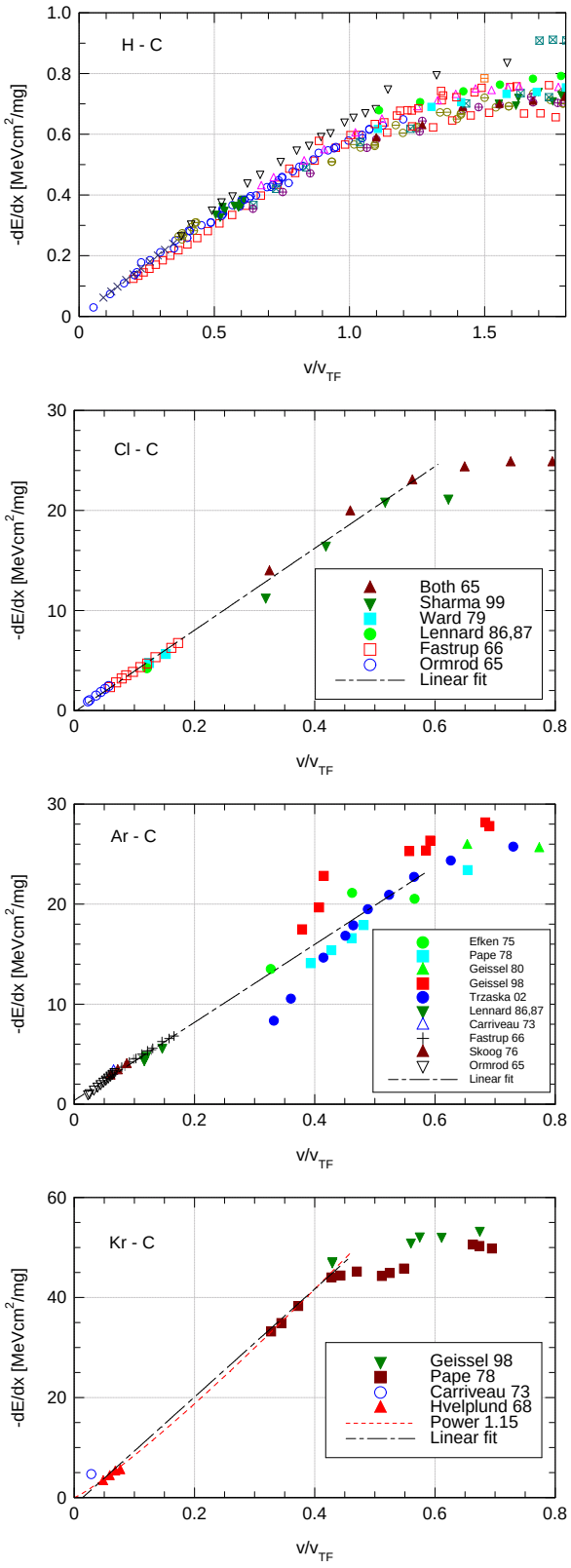

Figure 3: *Color on screen.* Same as figure 1 for H and Cl in C. Original data from [5, 26, 27, 33–43]. Listing of proton references in ref. [9].

4. Comparison with Theory

We find it appropriate to mention that the behavior found by Brown and Moak [7] is by no means unusual.

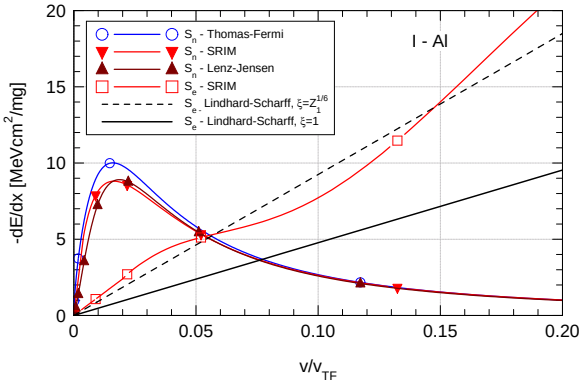

Figure 4: *Color on screen.* Calculated electronic and nuclear stopping cross sections for iodine in aluminium. Evaluated from [3] except for curves labeled SRIM [8].

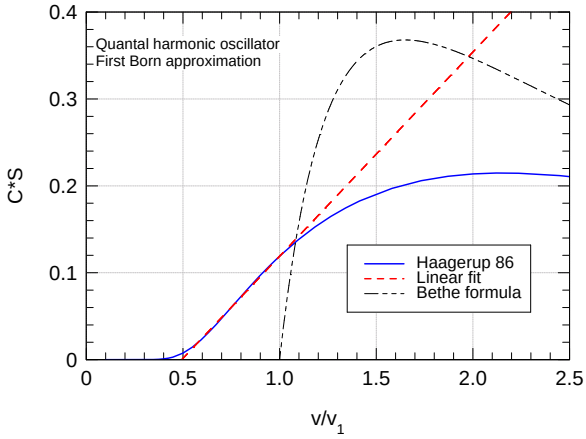

Figure 5: *Color on screen.* Stopping cross section of a harmonic-oscillator atom for a point charge in the first Born approximation according to ref. [45]. Abscissa unit $v_1 = \sqrt{\hbar\omega/2m}$. Ordinate unit $1/C = 8\pi Z_1^2 e^4/\hbar\omega_0$.

It is, in fact, representative of the acknowledged standard in this field, the Bethe theory. Figure 5 shows the stopping cross section of a harmonic-oscillator atom (resonance frequency ω_0) for a point charge, calculated in the first Born approximation by Haagerup and one of us [45], including all shell corrections but excluding projectile excitation, charge exchange and screening.

Unusual here is only the plot, which focuses on a velocity region where the first Born approximation is not very accurate, since it ignores Barkas-Andersen and other higher-order effects. There is a distinct quasi-linear regime in the velocity range $0.5v_1 \lesssim v \lesssim v_1$, pointing at an apparent threshold $0.5v_1$, and an effective threshold at $\sim 0.4v_1$, with $v_1 = \sqrt{\hbar\omega_0/2m}$. For orientation we also have included the standard Bethe formula, $S = (4\pi Z_1^2 e^4/mv^2)\ln(2mv^2/\hbar\omega_0)$, which ignores the shell correction and, therefore, indicates a real threshold.

Thus, the main reason for asking the questions in the introduction is the fact that the starting point of Brown and Moak was the Lindhard-Scharff formula rather than the Bethe theory.

The analysis of Lifschitz and Arista [15] is based on a

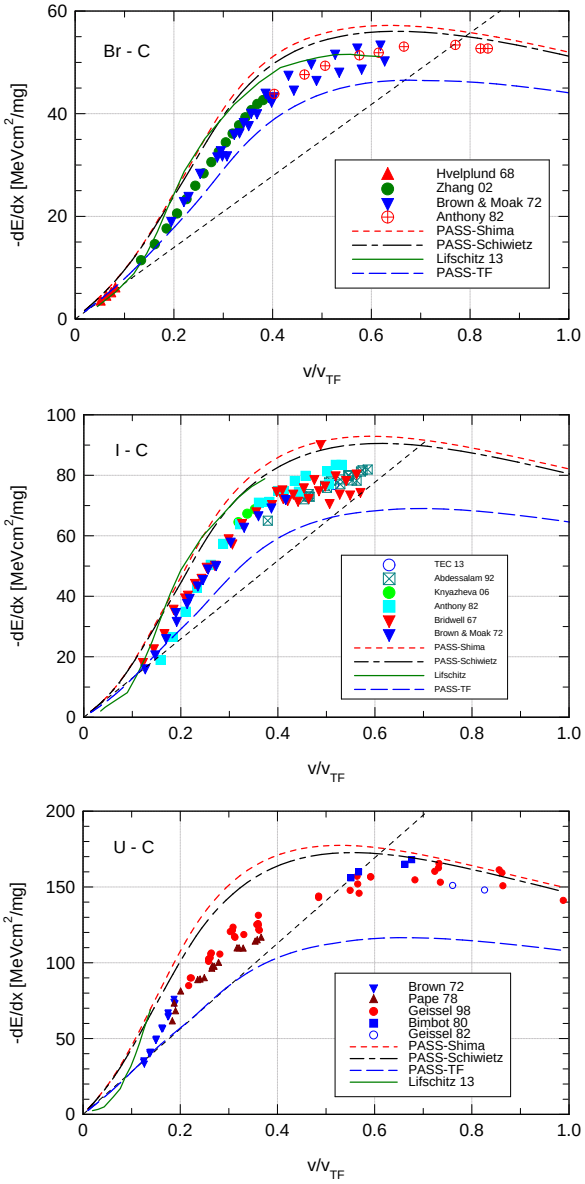

Figure 6: *Color on screen.* Experimental data from figure 1 compared with calculations by PASS for three different expressions for the equilibrium charge state, eq. (1), [46] and [47]. The curves labeled 'Arista' are quoted from ref. [15]. Straight dotted lines represent an inter- or extrapolated linear velocity dependence near $v = 0$.

code developed in refs. [48–50] which treats stopping as a quantal scattering problem between a screened ion and a free target electron.

The present theoretical analysis is based on binary stopping theory [51] as implemented in the PASS code [18]. Binary stopping theory is a modification of Bohr theory [52], allowing for shell and Barkas-Andersen corrections, projectile screening and projectile excitation, with input from electronic binding energies and dipole oscillator strengths. An inverse-Bloch correction is applied to extend the range of the theory into the Bethe regime, but this correction is not important within the parameter space

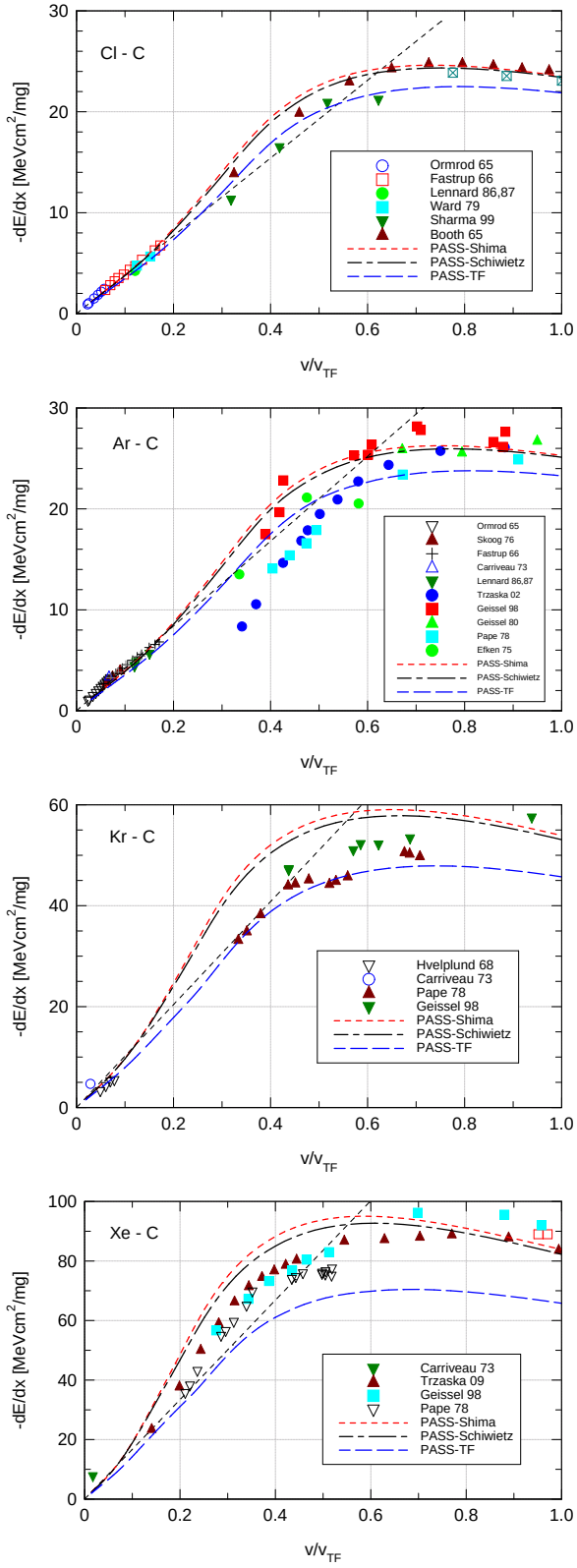

Figure 7: *Color on screen.* Same as figure 6 for Cl and Ar on carbon. Calculations from PASS. Dotted lines represent straight-line fits to experimental data.

covered here[1].

[1] An exception is the case of proton stopping, cf. figure 3, upper graph which, however, will not be analysed theoretically.

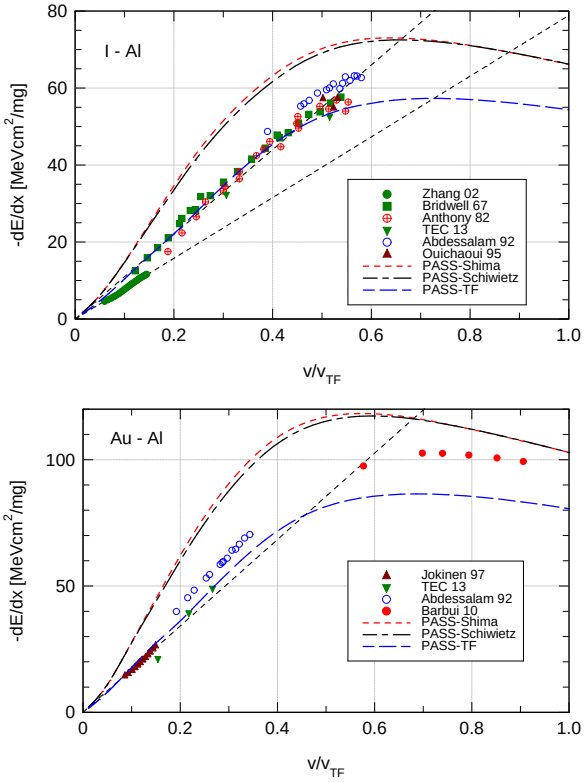

Figure 8: *Color on screen.* Same as figure 6 for gold and iodine ions in aluminium.

Options used in the present work are identical with those applied in ref. [1] with the exception that several expressions were adopted for the mean equilibrium charge, unlike in ref. [1], where we relied exclusively on what we call the standard Thomas-Fermi expression

$$q = Z_1 \left[1 - e^{-v/v_{\mathrm{TF}}} \right] . \qquad (1)$$

Figure 6 shows the data from figure 1 in conjunction with three results based on binary theory as well as those reported in ref. [15]. The results from binary theory (PASS code) differ solely in the adopted mean equilibrium charge, i.e. expressions from [46] and [47] in addition to eq. (1). It is seen that within the nominal range of validity of the binary theory, for $v > v_0$, all but two experimental data points lie between the predictions of the PASS code for Thomas-Fermi and Shima charge functions, respectively. Results based on the charge function from ref. [47] almost coincide with those found for Shima-charges. In earlier work concentrating on lighter ions [18] we found only a minor influence of the charge function on the stopping cross section. It is evident that the difference increases notably from Br to U ions, in agreement with ref. [53].

It is seen that the results of Lifschitz and Arista [15] lie close to those found by the PASS code with the Shima

or Schiwietz charge function. The three Lifschitz curves show a rather abrupt change in slope at $v/v_{TF} \sim 0.1$. This seems to match the experimental data in that velocity range very well, especially for Br-C, but tends to overestimate both magnitude and slope at higher velocities.

Figure 7 shows similar graphs for Cl, Ar, Kr and Xe in carbon. In accordance with previous conclusions [18], stopping cross sections for Cl and Ar are only weakly dependent on the charge function. Also for Kr and Xe ions the experimental data – which show considerable scatter – lie close to the arithmetic mean between the curves found for Thomas-Fermi and Shima-Schiwietz charge.

Figure 8 shows reasonably good agreement between the aluminium data from figure 2 and standard PASS calculations adopting Thomas-Fermi charge states, eq. (1). No calculations have been reported in ref. [15] for these systems nor for those in figure 7.

PASS results for Thomas-Fermi charge suggest the stopping maximum to lie close to $v/v_{TF} = 0.7$. This is consistent with the majority of the experimental data shown in the graphs, taking due account of the scatter. Conversely, PASS calculations with Shima or Schiwietz charge predict the stopping maximum do decrease slowly from $v/v_{TF} = 0.7$ to ~ 0.5 for Z_1 going from 17 to 92.

5. Analysis

Velocity-proportional stopping is expected whenever $v \ll v_e$, where v_e is a representative speed of a target electron[2]. Therefore, an initial slope in a stopping plot can be defined from a given theory, and from this we can judge whether curves bend upward or downward from there.

We see two obvious reasons why stopping cross sections may show a positive curvature after an initial straight-line behavior,

(I) Increasing contributions from inner target shells,

(II) Increasing ion charge.

In addition, Lifschitz and Arista [15] point at

(III) Variations in dynamic screening.

We look at these aspects separately.

5.1. Shell Effects

Figure 9, upper graph, shows the Thomas-Fermi stopping force for the Br-C system separated into contributions from three target shells (1s,2s,2p) as well as projectile excitation, electron capture and loss (PE). Also included are straight lines matched to the initial slope.

As was to be expected, the contribution from 2p electrons dominates over the entire velocity range covered by

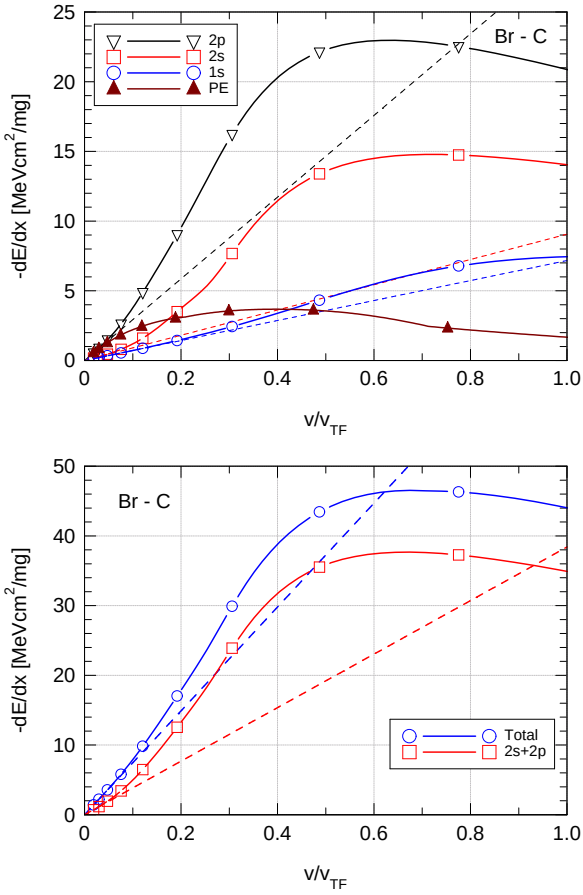

Figure 9: *Color on screen.* Upper graph: Calculated stopping force for Br in C separated into contributions from three target shells and projectile excitation, capture and loss (PE). PASS code, Thomas-Fermi charge eq. (1). Dashed lines extrapolated from initial slope. Lower graph: Partial sum 2s+2p compared with total.

the graph, but the ratio S_{2s}/S_{2p} rises from 0.3 at the low-v limit to 0.6 around the maximum.

Apart from this, the contributions from the target shells show a positive curvature which point at effects like (II) and (III) in the above classification. However, the PE contribution shows negative curvature which roughly compensates for the positive curvature of the leading target shell.

In the study of Lifschitz and Arista [15] the target was described as a homogeneous electron gas, and projectile excitation, electron capture and loss were ignored. The lower graph of figure 9 shows that this approximation, when implemented in the PASS code, together with the neglect of the 1s shell, gives rise to a slightly (20%) lower stopping cross section in the maximum. At the same time, a factor-of two underestimate of the initial slope is found. We assert that the neglect of projectile excitation, i.e., a contribution with a negative curvature, is the main reason for the excessively sharp rise of the stopping cross sections reported by Lifschitz and Arista [15].

Figure 10 shows a similar analysis for I-Al. A pronounced positive curvature is found for energy loss to

[2] Apparent threshold behavior observed in distinct collision systems primarily for proton bombardment [54, 55] is outside the scope of the present paper.

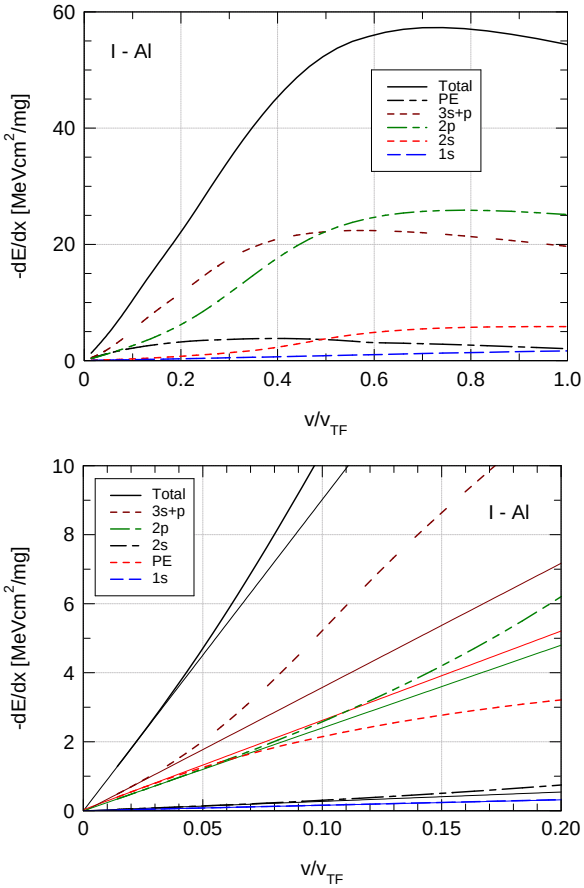

Figure 10: *Color on screen.* Same as Figure 9 for ionide in aluminium. The lower graph zooms on the regime $v/v_{TF} < 0.2$ and includes straight-line extrapolations (thin solid lines).

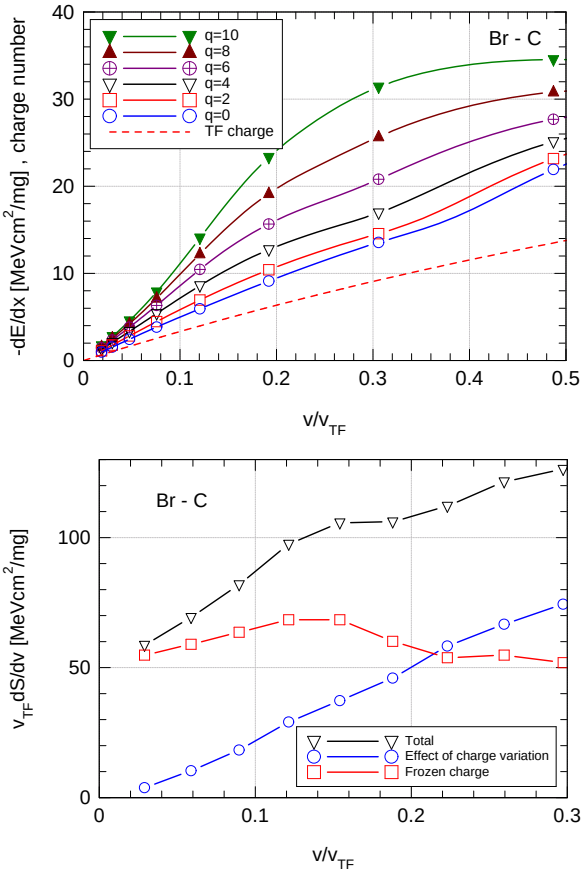

Figure 11: *Color on screen.* Variation of the stopping force with ion charge for BR-C, calculated by PASS code, Thomas-Fermi charge eq. (1) assumed. Upper graph: Frozen-charge stopping force for $q = 0, 2, 4, 6, 8, 10$ including projectile excitation. Variation of equilibrium stopping force split according to eq. (3), where the first term is labelled 'frozen charge' and the second 'effect of charge variation'.

3s+p electrons. This is, however, efficiently counteracted by a negative curvature in the contribution from projectile excitation. The result is quite close to a straight line through the origin.

5.2. Ion Charge

Expressing the stopping force by the stopping cross section S we may write

$$-\frac{dE}{dx} = NS = NS(q,v)|_{q=q(v)}\,, \qquad (2)$$

where $S(q,v)$ represents the velocity dependence of the stopping cross section at a frozen ion charge q, and $q(v)$ the equilibrium charge as a function of v. We may then look at the quantity

$$\frac{dS}{dv} = \frac{\partial S(q,v)}{\partial v}\bigg|_{q=q(v)} + \frac{\partial S(q,v)}{\partial q}\frac{dq(v)}{dv}. \qquad (3)$$

The matter is illustrated in figure 11 for Br-C. The upper graph shows frozen-charge stopping forces. All of them show an initial linear dependence, followed up by a more or less pronounced regime of negative curvature.

In the lower graph the two contributions making up eq. (3) are shown separately. The variation of the ion charge yields a monotonically increasing contribution, resulting in a positive curvature of the stopping force. The variation with v of the frozen-charge line shows ups and downs, indicating positive and negative curvature. The total result, however, shows a slope determined predominantly by the variation of the ion charge. Thus, apart from a quasilinear behavior around $0.15 \lesssim v/v_{TF} \lesssim 1.9$ this graph indicates positive curvature due to the variation of the ion charge up to $v/v_{TF} \simeq 0.3$.

5.3. Screening

Figure 12 shows a comparison between the stopping force for Br-C reported by Lifschitz and Arista [15] and two results from the PASS code. In order to ensure a fair comparison, PASS results ignore excitation of 1s target electrons as well as projectile excitation. The relevant charge state for comparison is the one by Schiwietz and Grande [47]. The standard Thomas-Fermi charge has only been included to mark the difference.

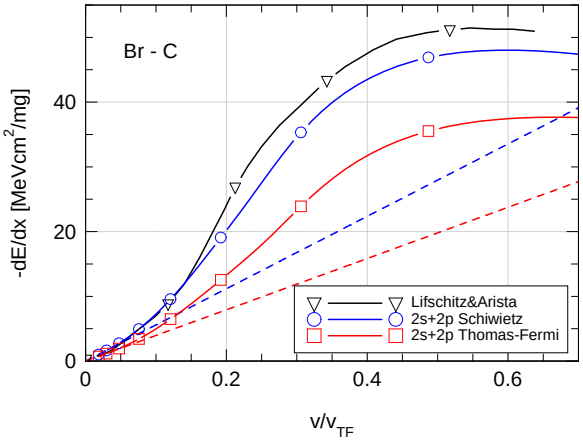

Figure 12: *Color on screen.* Stopping force for Br-C reported in ref. [15] compared to results from PASS for target excitation/ionization of 2s and 2p shells, projectile excitation and electron capture and loss ignored. Dotted lines extrapolated from the low-v behavior.

We find complete agreement between the curve from ref. [15] and the PASS result for Schiwietz charge up to $v/v_{TF} \lesssim 0.15$. This regime extends noticeably above the low-v (velocity-proportional) regime specified by dotted straight lines. For $1.5 \lesssim v/v_{TF} \lesssim 2.0$ we find a regime of slightly increased curvature in the result from ref. [15]. This is likely to indicate a difference in the screening functons used in the two models. There is also a difference between the two schemes in the way how scattering cross sections are calculated – classically or quantally – but that difference is known to show up most prominently at the low-v end.

Differences between the screening functions underlying the two schemes are specified in Appendix A. At this point we note that figure 12 shows that the practical consequences of these differences are rather minor. Note in particular that the two pertinent stopping forces differ only by a constant for $v/v_{TF} \gtrsim 0.2$. There is, however, a major difference in the underlying argument.

In the model of ref. [15], screening is a property of the electron gas and determined by a requirement of dynamic equilibrium in terms of a modified Friedel sum rule [48]. A weak point of this argument is the fact that unlike for the original (static) Friedel sum rule, the question of whether or not equilibrium actually can be achieved in the velocity range under consideration is unsolved.

In binary theory [51], screening enters as a way to model the effect of electron binding. The resulting dependence of the mean energy loss versus impact parameter coincides with the Bohr theory for distant collisions [56]. In addition to kinetic-energy transfer, binary theory also takes into account potential-energy transfer, which is ignored in the model of ref. [15].

In other words, in the form applied in the present study, binary theory models stopping in a sequence of ion-atom collisions[3], and dynamical screening has been excluded as a contributing feature. Dynamic screening could be introduced as an *additional* effect, but that has not been done here.

6. Discussion

Returning to the questions asked in the introduction we reiterate that velocity-proportional stopping is not a general feature supported by theoretical evidence for $v \gtrsim v_0$. This has also been concluded by Lifschitz and Arista [15].

While experimental evidence is somewhat ambiguous, theory points into the following classification of a stopping cross section into the regimes,

- An initial regime of velocity proportional stopping, typically[4] $v \ll v_0$,
- A regime of positive curvature caused by decreasing significance of atomic binding and increasing ion charge,
- This increase is strengthened by increasing contributions from inner target shells but weakened by decreasing significance of projectile excitation,
- There must be a turning point toward negative curvature. In view of the number of pertinent factors, a regime of almost zero curvature is feasible but not a general phenomenon.
- A possible influence of dynamic screening, emphasized by Lifschitz and Arista [15] is rather small, of the order of the difference between the curve marked by triangles and the one marked by circles in figure 12.
- Despite the neglect of the inner target shell and projectile excitation, estimates in ref. [15] overestimate experimental stopping forces. This is likely to indicate weaknesses in the employed screening radii.

Appendix A. Details on Screening

In the PASS code, screening functions enter classical scattering integrals governing the scattering of target electrons on a partially-stripped projectile ion. The PASS code operates with a potential

$$V(r) = -\frac{q_1 e^2}{r} e^{-r/a_{\rm ad}} - \frac{(Z_1 - q_2)e^2}{r} \chi\left(\frac{r}{a}\right), \quad \text{(A.1)}$$

where $a_{\rm ad} = v/\omega$ is the adiabatic radius, ω the resonance frequency of the respective shell, a an effective screening radius defined by

$$\frac{1}{a^2} = \frac{1}{a_{\rm ad}^2} + \frac{1}{a_{\rm sc}^2}, \quad \text{(A.2)}$$

[3] An exception is the case of aluminium, where 3s+p electrons are modeled as a Fermi gas

[4] As noted previously, the question of threshold behavior is left open here.

$$a_{\rm sc} = a_{\rm TF}\left(1 - \frac{q_1}{Z_1}\right), \qquad \text{(A.3)}$$

and $a_{\rm TF} = 0.8853 a_0/Z_1^{1/3}$ the Thomas-Fermi screening radius of a neutral atom. We operate with either Thomas-Fermi or Moliere screening functions for $\chi(r/a)$.

In ref. [15], screening functions enter the Schrödinger equation and differ from eq. (A.1) in two respects:

- In the first term on the right-hand side, the screening radius is determined by the requirement of neutrality, an extended Friedel sum rule [48].
- The second term on the right-hand side is assumed velocity-independent.

While the requirement of neutrality remains to be proven, we question the neglect of a velocity dependence in the second term: Dynamic screening applies to all moving charges, not only the nucleus but also its screening cloud.

Acknowledgments

Discussions with Nestor Arista are gratefully acknowledged. This work has been supported by the Carlsberg foundation.

[1] ICRU, *Stopping of ions heavier than helium*, vol. 73 of *ICRU Report* (Oxford University Press, Oxford, 2005).
[2] J. Lindhard and M. Scharff, Phys. Rev. 124 (1961) 128.
[3] J. Lindhard, M. Scharff and H. E. Schiøtt, Mat. Fys. Medd. Dan. Vid. Selsk. 33 no. 14 (1963) 1.
[4] J. Lindhard, V. Nielsen, M. Scharff and P. V. Thomsen, Mat. Fys. Medd. Dan. Vid. Selsk. 33 no. 10 (1963) 1.
[5] B. Fastrup, P. Hvelplund and C. A. Sautter, Mat. Fys. Medd. Dan. Vid. Selsk. 35 no. 10 (1966) 1.
[6] C. D. Moak and M. D. Brown, Physical Review 149 (1966) 244.
[7] M. D. Brown and C. D. Moak, Phys. Rev. B 6 (1972) 90.
[8] J. F. Ziegler, *Particle interactions with matter* (2012), URL `www.srim.org`.
[9] H. Paul, *Stopping power graphs* (2013), URL `www.exphys.uni-linz.ac.at/stopping/`.
[10] E. Fermi and E. Teller, Phys. Rev. 72 (1947) 399.
[11] J. Lindhard, Mat. Fys. Medd. Dan. Vid. Selsk. 28 no. 8 (1954) 1.
[12] J. Lindhard and A. Winther, Mat. Fys. Medd. Dan. Vid. Selsk. 34 no. 4 (1964) 1.
[13] O. B. Firsov, Zh. Eksp. Teor. Fiz. 36 (1959) 1517, [Engl. transl. Sov. Phys. JETP **9**, 1076-1080 (1959)].
[14] Y. A. Teplova, V. S. Nikolaev, I. S. Dimitriev and L. N. Fateeva, Zh. Eksp. Teor. Fiz. 42 (1962) 44, [Engl. transl. Sov. Phys. JETP **15**, 31-41 (1962)].
[15] A. F. Lifschitz and N. R. Arista, Nucl. Instrum. Methods B 316 (2013) 245.
[16] P. Sigmund, Europ. Phys. J. D 47 (2008) 45.
[17] V. Kuzmin and P. Sigmund, Nucl. Instrum. Methods B 269 (2011) 817.
[18] P. Sigmund and A. Schinner, Nucl. Instrum. Methods B 195 (2002) 64.
[19] P. Hvelplund and B. Fastrup, Phys. Rev. 165 (1968) 408.
[20] Y. Zhang, G. Possnert and W. J. Weber, Appl. Phys. Lett. 80 (2002) 4662.
[21] J. M. Anthony and W. A. Lanford, Phys. Rev. A 25 (1982) 1868.
[22] L. B. Bridwell, L. C. Northcliffe, S. Datz, C. D. Moak and H. O. Lutz, Phys. Rev. 159 (1967) 276.
[23] G. N. Knyazheva, S. V. Khlebnikov, E. M. Kozulin, T. E. Kuzmina, V. G. Lyapin, M. Mutterer, J. Perkowski and W. H. Trzaska, Nucl. Instrum. Methods B 248 (2006) 7.
[24] M. Abdesselam, J. Stoquert, G. Guillaume, M. Hageali, J. Grob and P. Siffert, Nucl. Instrum. Methods B 72 (1992) 293.
[25] N. P. Barradas and A. Simon, IAEA (2013).
[26] H. Pape, H. G. Clerc and K. H. Schmidt, Z. Phys. A 286 (1978) 159.
[27] H. Geissel and C. Scheidenberger, Nucl. Instrum. Methods B 136-8 (1998) 114.
[28] R. Bimbot, D. Gardès, H. Geissel, T. Kitahara, P. Armbruster, A. Fleury and F. Hubert, Nucl. Instrum. Methods 174 (1980) 231.
[29] H. Geissel, GSI-Report 82-12 (1982) 21.
[30] S. Ouichaoui, L. Rosier, E. Hourany, R. Bimbot, N. Redjdal and H. Beaumevieille, Nucl. Instrum. Methods B 95 (1995) 463.
[31] J. Jokinen, Nucl. Instrum. Methods B 124 (1997) 447.
[32] M. Barbui, D. Fabris, M. Lunardon, S. Moretto, G. Nebbia, S. Pesente, G. Viesti, M. Cinausero, G. Prete, V. Rizzi, K. Hagel, S. Kowalski, J. B. Natowitz, L. Qin, R. Wada and Z. Chen, Nucl. Instrum. Methods B 268 (2010) 20.
[33] J. H. Ormrod, J. R. MacDonald and H. E. Duckworth, Can. J. Phys. 43 (1965) 275.
[34] W. Booth and I. S. Grant, Nucl. Phys. 63 (1965) 481.
[35] G. W. Carrivea, G. Beauchemin, E. J. Knystautas, E. H. Pinnington and R. Drouin, Phys. Lett. A 46 (1973) 291.
[36] B. Efken, D. Hahn, D. Hilscher and G. Wüstefeld, Nucl. Instrum. Methods 129 (1975) 219.
[37] R. Skoog and K. Augenlicht-Jakobsson, Radiat. Eff. 27 (1976) 143.
[38] D. Ward, H. R. Andrews, I. V. Mitchell, W. N. Lennard, R. B. Walker and N. Rud, Can. J. Phys. 57 (1979) 645.
[39] H. Geissel, P. Armbruster, T. Kitahara, G. Kraft, H. Spieler and K. Güttner, Nucl. Instrum. Methods 170 (1980) 217.
[40] W. N. Lennard, H. Geissel, D. Jackson and D. Phillips, Nucl. Instrum. Methods B 13 (1986) 127.
[41] W. N. Lennard and H. Geissel, Nucl. Instrum. Methods B 27 (1987) 338.
[42] A. Sharma, S. Kumar, S. K. Sharma, N. Nath, V. Harikumar, A. P. Pathak, L. N. S. P. Goteti, S. K. Hui and D. K. Avasthi, J. Phys. G 25 (1999) 135.
[43] W. H. Trzaska, V. Lyapin, T. Alanko, M. Mutterer, J. Räisänen, G. Tjurin and M. Wojdyr, Nucl. Instrum. Methods B 195 (2002) 147.
[44] L. G. Glazov and P. Sigmund, Nucl. Instrum. Methods B 207 (2003) 240.
[45] P. Sigmund and U. Haagerup, Phys. Rev. A 34 (1986) 892.
[46] K. Shima, T. Ishihara and T. Mikumo, Nucl. Instrum. Methods 200 (1982) 605.
[47] G. Schiwietz and P. L. Grande, Nucl. Instrum. Methods B 175-177 (2001) 125.
[48] A. F. Lifschitz and N. Arista, Phys. Rev. A 57 (1998) 200.
[49] N. R. Arista, Nucl. Instrum. Methods B 195 (2002) 91.
[50] N. R. Arista and A. F. Lifschitz, Adv. Quantum Chem. 45 (2004) 47.
[51] P. Sigmund and A. Schinner, Europ. Phys. J. D 12 (2000) 425.
[52] N. Bohr, Philos. Mag. 25 (1913) 10.
[53] A. Fettouhi, H. Geissel, A. Schinner and P. Sigmund, Nucl. Instrum. Methods B 245 (2006) 22.
[54] R. Golser and D. Semrad, Phys. Rev. Lett. 66 (1991) 1831.
[55] M. Draxler, S. Chenakin, S. Markin and P. Bauer, Phys. Rev. Lett. 95 (2005).
[56] P. Sigmund, Phys. Rev. A 56 (1997) 3781.